Atmospheric Research 102 (2011) 300–310

Contents lists available at ScienceDirect

Atmospheric Research

journal homepage: www.elsevier.com/locate/atmos

Investigation of the 3-D actinic flux field in mountainous terrain

J.E. Wagner [a,*], F. Angelini [b], M. Blumthaler [c], M. Fitzka [a], G.P. Gobbi [b], R. Kift [d], A. Kreuter [c], H.E. Rieder [e], S. Simic [a], A. Webb [d], P. Weihs [a]

[a] Institute for Meteorology, University of Natural Resources and Life Sciences, Peter-Jordan-Straße 82, A-1190 Vienna, Austria
[b] Institute of Atmospheric Sciences and Climate, Rome, Italy
[c] Division for Biomedical Physics, Innsbruck Medical University, Innsbruck, Austria
[d] School of Earth, Atmospheric and Environmental Sciences, University of Manchester, Manchester, United Kingdom
[e] Institute for Atmospheric and Climate Science, ETH Zurich, Zurich, Switzerland

ARTICLE INFO

Article history:
Received 15 July 2010
Received in revised form 14 July 2011
Accepted 20 July 2011

Keywords:
Actinic flux
Radiative transfer
Monte Carlo Model
UV radiation
Surface albedo
Spectroradiometry
Photolysis frequencies

ABSTRACT

During three field campaigns spectral actinic flux was measured from 290–500 nm under clear sky conditions in Alpine terrain and the associated O3- and NO2-photolysis frequencies were calculated and the measurement products were then compared with 1-D- and 3-D-model calculations. To do this 3-D-radiative transfer model was adapted for actinic flux calculations in mountainous terrain and the maps of the actinic flux field at the surface, calculated with the 3-D-radiative transfer model, are given. The differences between the 3-D- and 1-D-model results for selected days during the campaigns are shown, together with the ratios of the modeled actinic flux values to the measurements. In many cases the 1-D-model overestimates actinic flux by more than the measurement uncertainty of 10%. The results of using a 3-D-model generally show significantly lower values, and can underestimate the actinic flux by up to 30%. This case study attempts to quantify the impact of snow cover in combination with topography on spectral actinic flux. The impact of snow cover on the actinic flux was ~25% in narrow snow covered valleys, but for snow free areas there were no significant changes due snow cover in the surrounding area and it is found that the effect snow-cover at distances over 5 km from the point of interest was below 5%. Overall the 3-D-model can calculate actinic flux to the same accuracy as the 1-D-model for single points, but gives a much more realistic view of the surface actinic flux field in mountains as topography and obstruction of the horizon are taken into account.

1. Introduction

Ultraviolet spectroradiometry has grown in importance during the last few decades due to the increasing need for high quality measurements of UV radiation in areas such as medicine, e.g. Melamed et al. (2008), atmospheric chemistry, e.g. Raff and Finlayson-Pitts (2010), and material science, e.g. Kaczmarek et al. (2009), for high-quality measurements of UV radiation (UVR). There are numerous case studies and long-term investigations into global solar irradiance, defined as the sum of direct and diffuse irradiance coming from the upper hemisphere, received on a flat horizontal surface (e.g. McKenzie et al. (1993), Pribullova and Chmelik (2008)). While irradiance is the standard quantity for solar radiation, measurements of actinic flux have become increasingly popular enabled by the development of suitable input optics (Bais et al. (2001), Hofzumhaus et al. (2002)). Actinic flux represents the radiation which is received at a point with each photon being assigned with the same weight irrespective of incident direction. Recent investigations in the actinic flux have used airborne measurements and model calculations of actinic flux (Palancar et al. (2011), Bierwirth et al. (2010)) and for less complex situations (low surface albedo, clear sky conditions, simple topography) the agreement between models and measurements is within 5–10%, but for

* Corresponding author. Tel.: +43 1476545625; fax: +43 1476545610.
E-mail address: jochen.wagner@boku.ac.at (J.E. Wagner).

0169-8095/$ – see front matter © 2011 Elsevier B.V. All rights reserved.
doi:10.1016/j.atmosres.2011.07.008

more complex situations (variable surface albedo, partial cloud cover, complex topography) deviations are much larger (Bais et al. (2003), Thiel et al. (2008)). Spectral actinic flux can be integrated to derive photolysis frequencies J, which describe specific photochemical dissociation processes. Therefore the actinic flux is an elementary quantity for atmospheric photochemistry. However, measuring actinic flux is more difficult than irrradiance, since a detector with uniform response characteristics over one hemisphere ($2\pi\ sr$) is needed (Volz-Thomas et al. (1996) and Junkermann et al. (1989)).

Spectroradiometers with suitable input optics are the most accurate instruments for measuring the spectrally resolved UV actinic flux (Bais et al. (2001). As ground-based high quality spectral UV actinic flux measurements are only available for a small number of research sites worldwide, different calculation methods have been developed over the last three decades (e.g. Stamnes et al., 1988). 1-D radiative transfer models like DISORT (Stamnes et al., 1988) or POLRADTRAN (Evans and Stephens, 1991) have been popular for about two decades while 3-D radiative transfer models (e.g., Cahalan et al., 2005) are a more recent development. A comprehensive intercomparison of 3-D radiative transfer models is available at http://i3rc.gsfc.nasa.gov/I3RC-intro.html.

The UV actinic flux under clear sky conditions, is determined largely by solar zenith angle and total column ozone (Feister and Grewe, 1995a, Burrows, 1997, Kerr, 2003), but the aerosol optical depth and the ground albedo also have a significant impact. Investigations into the impact of surface albedo on the radiation field were conducted by Blumthaler and Ambach (1988), Kylling et al. (2000), Schwander et al. (1999) and Weihs et al. (2001). All these studies suggest that surface albedo, especially in the presence of snow, has a significant influence on the UVR field. Actinic flux can be enhanced significantly more strongly than irradiance by surface albedo because of its angle dependence (Madronich, 1987). Other studies have shown that the UVR is significantly affected by variations in atmospheric aerosols especially in urban areas (Jaroslawski , 2005, Kylling et al., 1998). Furthermore the impact of both aerosols and surface albedo on UVR for a particular mountain site (Sonnblick 3106 m) has been investigated (Weihs et al., 1999, Simic et al., 2008,Rieder et al., 2010). The interplay of mountainous topography and high surface albedo with respect to spectral irradiance at 340 nm was studied by Kylling and Mayer (2001) using measurements and 3-D-model simulations. Lenoble et al. (2004) also studied the enhancement of the UV irradiance due to snow cover on the ground in mountainous terrain. Both studies report an enhancement due to snow cover of about 25% for clear sky situations. General aspects of 3-D-radiative transfer are discussed by Bass et al. (2010) and Deutschmann et al. (2011). Degünther et al. (1998) used a 3-D-model to calculate UV irradiance under cloud-free conditions in mountainous, partly snow-covered terrain and reported a large horizontal impact of snow-covered surface with significant enhancements of up to 3% due to ground albedo affects from more than 40 km away from the measurement site. It is not straight forward to convert UV irradiance to UV actinic flux but Webb et al. (2002) and Kylling et al. (2003) have developed conversion algorithms. The conversion works better at certain low solar zenith angles and information on the sky situation (clear sky or cloudy) is also crucial. However modeling of UV spectral actinic flux in mountainous areas, especially in the presence of snow, is complex and still poses a scientific challenge. So far the influence of snow and topography on surface actinic flux has not been quantified, a problem adressed by this work.

We compare measurements with 1-D and 3-D-model calculations of spectral actinic flux at 305, 310, 324 and 380 nm. In addition photolysis frequencies for ozone (O3) and nitrogen dioxide (NO2) can be calculated from both modeled and measured spectra. These two reactions are regarded as the most important photodissociation reactions in the troposphere. Photodissociation of ozone ($O_3+hv\rightarrow O_2+O(^1D)$) generates an exited oxygen atom which can react with water to give the hydroxyl radical ($O(^1D)+H_2O)\rightarrow 2OH$). The hydroxyl radical is central to atmospheric chemistry as it initiates the oxidation of hydrocarbons in the atmosphere and so acts as a detergent. Photodissociation of nitrogen dioxide ($NO_2\rightarrow NO+O$) is a key reaction of tropospheric ozone ($O+O_2\rightarrow O_3$). Quantifying the impact of surface albedo and topography on actinic fluxes under cloud-free conditions, in Alpine terrain is thus an important contribution to a better understanding of the chemistry in such regions.

2. Material and methods

2.1. Ground-based measurements

Ground-based measurements were performed during two campaigns near Innsbruck, in late summer 2007 (2nd September to 22nd September) and in late winter 2008 (19th February to 6th March) and one measurement campaign in spring 2008 (29th April to 9th May) near Sonnblick. It was the intention to perform measurements first for snow-free conditions in September and then for snow-covered conditions in February and May. Unfortunately due to the presence in Innsbruck region of more than the usual snow in September and less snow in February, the resulting differences in snowline were only small (1900 m in September and between 1300 and 1700 m in February). Prior to each campaign an instrument intercomparison was performed. Differences of less than 5% were found between the reference instrument from the Medical University Innsbruck and the instruments from the two other participating parties, the University of Manchester and the University of Natural Resources and Life Sciences (BOKU), Vienna.

During the first campaign, spectral UV actinic flux was measured at two stations (see Table 1 and Fig. 1 for details) using two Bentham DTM 300 spectroradiometers (Bernhard and Seckmeyer, 1999). The entrance optic is designed such that photons incident from all angles are equally represented — there is no significant angular dependence (Hofzumahaus et al., 1999). The Innsbruck station (Inn) is situated on a roof in the city center of Innsbruck and represents a typical valley site. The second station, Hafelekar (*Haf*) is only 7 km away from the Innsbruck site, but on top of the mountain range North of Innsbruck (Nordkette). During the second campaign in Innsbruck, measurements using Bentham DTM 300s were carried out at Innsbruck and Hafelekar sites and using a Bentham DM 150 at an additional site in Lans. This site is about 6 km away from Innsbruck, situated about 250 m above the valley bottom.

Table 1
Information on ground-based stations used in this study.

Measurement site (abbreviation)	Instrument	Latitude	Longitude	Altitude
Innsbruck (*Inn*)	BENTHAM DTM300	47.26428°N	11.38511°E	616 m a.s.l.
Lans (*Lan*)	BENTHAM DM150	47.24544°N	11.43175°E	833 m a.s.l.
Hafelekar (*Haf*)	BENTHAM DTM300	47.31267°N	11.38386°E	2275 m a.s.l.
Bodenhaus (*Bod*)	BENTHAM DM150	47.09947°N	12.99575°E	1296 m a.s.l.
Kolm-Saigurn (*Kol*)	BENTHAM DTM300	47.06822°N	12.98406°E	1600 m a.s.l.

During the measurement campaign near Sonnblick, UV actinic flux was measured at two sites Bodenhaus (*Bod*) and Kolm-Saigurn (*Kol*) (see Table 1 and Fig. 2 for details) with two Bentham spectroradiometers. *Bod* and *Kol* are typical valley stations situated in a steep valley stretching from the Alpine main ridge northward with Kol beeing furthest into the valley and thus experiencing the greatest obstruction of the horizon.

At all stations, Bentham spectroradiometers were used to measure actinic flux from the upper hemisphere (solid angle 2 π) spectrally from 290 nm to 500 nm in 30 min intervalls. The stepwidth is 0.5 nm and the bandwidth (FWHM) is 0.77 nm. The instruments are calibrated regularly to a NIST (National Institute of Standards and Technology) calibrated 1000 W lamp. For further details on the instruments see Erb (1996). We used the instant values at the chosen wavelength from spectra obtained by the Bentham instruments. As the slit function varies between the instruments this has to be taken into account when comparing measurements from different sites, or with the model. The measured data were transformed to represent those from the same instrument but a standard triangular slit function with a 1 nm full width at half maximum (FWHM) using the ShicRIVM algorithm (Slaper et al., 1995). This removes characteristic instrumental differences and standardizes the comparison with model data.

Aerosol vertical distribution was determined by continuous lidar ceilometer observations with a VAISALA LD-40 (Angelini et al., 2009), while sample profiles where acquired by a polarization lidar (Gobbi et al., 2003). Both measurements were performed at *Inn* station. In addition direct sun irradiance measurements with a sun filter photometer were used to determine the aerosol optical depth on clear sky days. The wavelengths of the filters are 368, 412, 501 and 862 nm. The Ångstrøm coefficient β and the exponent α (Ångstrøm (1929)) are calculated by regression for the wavelength range 368–501 nm. During the days analyzed, aerosol optical depth was rather low, with the highest values being seen on 16th September (Table 2). However, even on 16th September the aerosol effect is rather small and is considered to be almost negligible (~5% at 324 nm and less for other wavelengths).

Total column ozone was measured with a Brewer Spectrophotometer at Sonnblick observatory and compared with data from Arosa (Switzerland) and Hohenpeissenberg (Germany). There were no significant differences found in total column ozone between these three stations on the days analyzed. Therefore measurements taken at Sonnblick are considered accurate enough for use in the Sonnblick and Innsbruck area. This is supported by Schmalwieser et al. (2008) who estimated the average difference in total column ozone between Innsbruck and Sonnblick to be on average less then 7%.

To estimate the surface albedo, observations of the snowline were used. The snowline was observed by eye and also classed as either a north- or south facing slope. We also tried to use satellite data to determine snow-covered areas, but this approach did not work well, because of the coarse resolution of the satellite data (500 m) in comparison with the model resolution (50 m). The difference in snowline between south-facing and north-facing slopes is largest on 24th February due to the warm and sunny conditions on the previous days, whereas there is no difference on 16th September (Table 2).

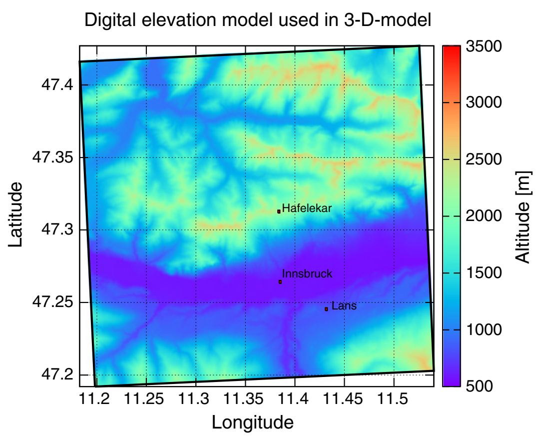

Fig. 1. The digital elevation map used within the 3-D-radiative transfer model is shown for Innsbruck section. The three measurement sites are also shown (see text for details).

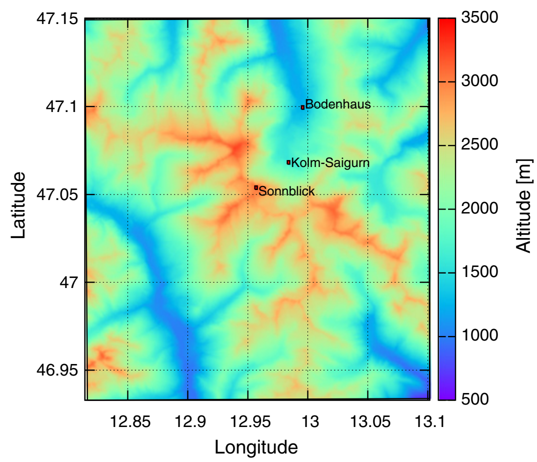

Fig. 2. Same as 1 but for the Sonnblick section. The two measurement sites Kolm-Saigurn and Bodenhaus and additionally the location of the Sonnblick observatory is marked.

Table 2
Input parameters for the the 3-D-models (altitude, solar zenith angle (SZA), time, total column ozone (ozone), albedo, Ångstrøm exponent and coefficient (α and β) and height of snowline (snowline). sza, azimuth and time are not dependent on the station (Inn - Innsbruck station, Haf - Hafelekar station, Lan - Lans station, Bod - Bodenhaus station, Kol - Kolm-Saigurn station),but on the modeled wavelength since the measurement of a spectrum lasts about 10 min (first value was used for 305 nm run, second value for 380 nm run). There are two values for surface albedo and snowline for the 3-D-model, first for snow-covered areas and second for snow-free areas and first value for the south-facing slopes and second for the north-facing slopes, respectively. Bold values indicate input parameter for both 1-D and 3-D-models, italics (in brackets) indicate input parameter for the 1-D-model.

Date	16.09.2007		24.02.2008			07.05.2008	
Station	*Inn*	*Haf*	*Inn*	*Lan*	*Haf*	*Bod*	*Kol*
Altitude [*m*]	576(*616*)	2278(*2275*)	576(*616*)	829(*833*)	2278(*2275*)	1288(*1296*)	1595(*1600*)
SZA [°]	**44.60 - 44.63**		**56.92 - 56.91**			**29.66 - 29.72**	
Azimut [°]	182.69 - 183.76		173.54 - 173.83			186.04 - 187.47	
Time [*UTC*]	**11:17–11:20**		**11:16–11:17**			**11:17–11:20**	
Ozone [*DU*]	**276**	**271**	**265**	**265**	**260**	**349**	**349**
Albedo	0.6/0.03(*0.14*)		0.7/0.03(*0.32*)			0.7/0.03(*0.58*)	
α	**1.4**	**1.4**	**1.1**	**1.1**	**1.1**	**1.08**	**1.08**
β	**0.060**	**0.024**	**0.020**	**0.016**	**0.004**	**0.022**	**0.028**
Snowline [*m*]	1900/1900		1700/1300			1700/1400	

For the snow-covered areas a surface albedo of 0.7 (surface partly covered with fresh snow) is assigned. For 16th September we assigned a value of 0.6 to allow for the presence of older snow following suggestions by Simic et al. (2005). For the 7th May and 24th February in the presence of relatively fresh snow the albedo for snow-covered areas was estimated to be 0.7 and for snow-free areas, an albedo of 0.03 was used. The albedo values used come from the findings of Feister and Grewe (1995b). Also it should be noted that Feister and Grewe (1995b) reported only a small wavelength dependence of the surface albedo for polluted snow and therefore the same value is used for all wavelengths.

2.2. Modeling

2.2.1. 1-D-radiative transfer model SDISORT

The libRadtran software package (http://libradtran.org/doku.php) was used to calculate spectral UV actinic flux and photolysis frequencies. This package consists of a set of programs to perform radiative transfer calculations using the UVSPEC interface (Mayer and Kylling, 2005) to run the SDISORT model (Dahlback and Stamnes, 1991). The SDISORT model is a well tested model used in the UV community being relatively easy to use and fast in terms of computation time. Although 1-D-models cannot take into account the effect of the local terrain, they have produced good results in several intercomparisons, of actinic flux in homogeneous areas (Kylling et al., 2005). These models use numerical methods to solve the radiative transfer equation and are mainly limited by knowledge of the properties of the Earth's atmosphere used in the model run. The SDISORT radiative transfer solver was run here using six streams. The spectral actinic flux was calculated using 1 nm steps and convolved with a triangular slit function with a FWHM = 1 nm. The ATLAS 3 extraterrestrial solar spectrum with 1 nm resolution was used and Sun-Earth distance corrections were applied. The AFGL (Air Force Geophysics Laboratory) mid-latitude profiles (Anderson et al. (1986)) were used for ozone, temperature and air pressure. The ozone profile was scaled according to total column ozone derived from Brewer measurements at Sonnblick. The 532 nm aerosol extinction profile was measured by the polarization lidar and scaled according to the 532 nm aerosol optical depth obtained by interpolation of consecutive sunphotometer aerosol optical depths (Langley method). We ran the 1-D-model using the input information indicated in Table 2. In the model the mountain top station (Hafelekar) was treated as a point above the surface. The surface height used in the 1-D-model is the average surface height of the 3-D-model domain (Fig. 1), e.g. 1386 m, and the height of the point is the actual height (Table 1, e.g. Hafelekar - 2275 m). This is the most realistic approach within a 1-D-model. To estimate 3-D-effects, another calculation with the 1-D-model was performed. We ran the 1-D-model individually for all $2.6*10^5$ pixels of the 3-D-model domain using the same surface height and surface albedo as in the 3-D-model. Finally the results were compared with the outcome of the 3-D-model (Fig. 9).

2.2.2. 3-D-radiative transfer model GRIMALDI

In comparison to 1-D models, 3-D models reproduce the radiation field more realistically in mountainous terrain as they allow to consider shadowing effects and reflections from tilted surfaces. A disadvantage of 3-D radiative transfer codes is that the computation time is much longer than for 1-D models. In this study, radiative transfer calculations were performed using the 3-D Monte Carlo model GRIMALDI (Scheirer and Macke, 2001). A detailed model description is also given in Scheirer and Macke (2003). GRIMALDI uses a Monte Carlo method for its 3-D-radiative transfer model and in the rest of the paper will be referred as the 3-D-model. Control runs of the 3-D-model without topography show an agreement of $\pm 5\%$ with the 1-D-model. Furthermore GRIMALDI (note, here referred to as UNIK) took part in an international Intercomparison of 3D Radiation Codes (Cahalan et al., 2005). We applied periodic conditions, with photons leaving the model domain at one side and entering the model domain at the opposite side. Two different model domains were used characterizing the area of investigation of the different field campaigns. The Innsbruck model domain has the size of x = 26 km, y = 25 km, z = 40 km and the Sonnblick model domain x = 21.75 km, y = 24.1 km, z = 40 km. The horizontal resolution was 50 m and the vertical resolution 200 m in both domains. Input data for total column ozone, the aerosol optical depth and vertical profiles of both are identical to the values used in the 1-D-model calculations. For this study two major changes to GRIMALDI model code were made.

First the model terrain was incorporated using a digital elevation map with a horizontal resolution of 50 m (Figs. 1 and 2) which also takes into account the inclination of the surface. Therefore it is possible to model the 3-D-radiation field much more realistically than in the 1-D-approach.

The second major change in the code of the GRIMALDI model is related to the actinic flux calculations. For calculating irradiance within the model it is adequate to count "photons" on a surface, but actinic flux is more complex. Therefore to calculate actinic flux, photons are counted on the surface of a cuboid. To convert photon numbers to actinic flux one has to take the geometry and the surface area of each pixel into account to calculate a "projected surface". The conversion from photon number to actinic flux is described in detail in Appendix A.

For each wavelength (305, 310, 324 and 380 nm) ten individual 3-D model runs were performed with 10^8 "photons" using input parameters indicated in Table 2. The final result was calculated using the mean of the ten model runs. With this approach, it is assured, that the numerical uncertainty is well below 5%. As a rule of thumb the CPU-time for one model run with 10^8 "photons" is about 36 h, therefore we ran the simulations in parallel on a computer cluster with 15 processors and obtained a calculation using 10^9 "photons" within about 24 h.

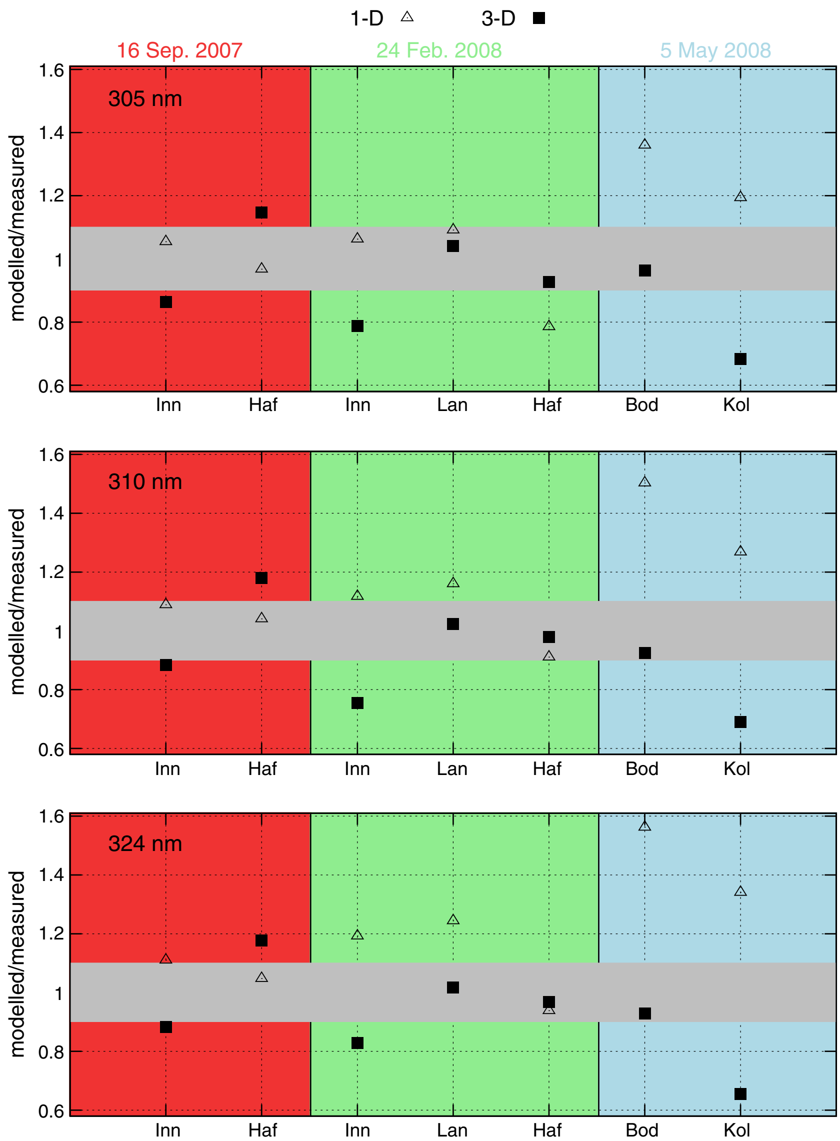

Fig. 3. Ratio of 1-D- and 3-D-model calculations to the measured value closest to noon (see legend at the top and Table 2). Top - 305 nm, center - 324 nm, bottom - 380 nm. The gray area marks the measurement uncertainty of ±10%. Ratios are calculated for the Innsbruck station (Inn) and Hafelekar station (Haf) on 16/09/2007, Inn, Lans station (Lan) and Haf on 24/02/2008 and Kolm-Saigurn station (Kol) and Bodenhaus station (Bod) on 05/07/2008 (see Figs. 1 and 2 for position of the stations).

2.2.3. Determination of the photolysis frequencies

To obtain photolysis frequencies from spectral actinic flux measurements and 1-D-model calculations the following approach was used. The O3-photolysis frequencies were calculated from spectral actinic flux between 290 nm and 340 nm, NO2-photolysis frequencies are calculated using spectral actinic flux between 290 nm and 420 nm. Photolysis frequencies J are derived by numerical integration of Eq. (1) using 1 nm steps.

$$J = \int \sigma(\lambda)\phi(\lambda)F_{\lambda}(\lambda)d\lambda \qquad (1)$$

Here $\sigma(\lambda)$ denotes quantum yield, $\phi(\lambda)$ absorption cross section and $F_{\lambda}(\lambda)$ the photon flux. Absorption cross sections and quantum yield data for a temperature of 0 °C were taken from the NASA Panel for Data Evaluation (http://jpldataeval.jpl.nasa.gov, Paur and Bass, 1985). To reduce computation time, we applied a slightly different method for 3-D-model calculations. We did not perform single calculations for each wavelength but instead just one calculation each for photons from two different wavebands (between 290 and 340 nm (O3 - photolysis) and between 290 and 420 nm (NO2 - photolysis)) was performed. For this calculation the contribution of each wavelength to the photolysis frequencies has to be determined in advance. This is achieved by multiplication of the spectral extraterrestrial irradiance with spectral absorption cross section and quantum yield. According to this value (between 0 and 1), 109 “photons” are distributed in 1 nm steps. The maximum impact and thus “photon” number occurs at 290 nm for O3 – photolysis and at 378 nm for NO2 – photolysis. Now these “photons” equally

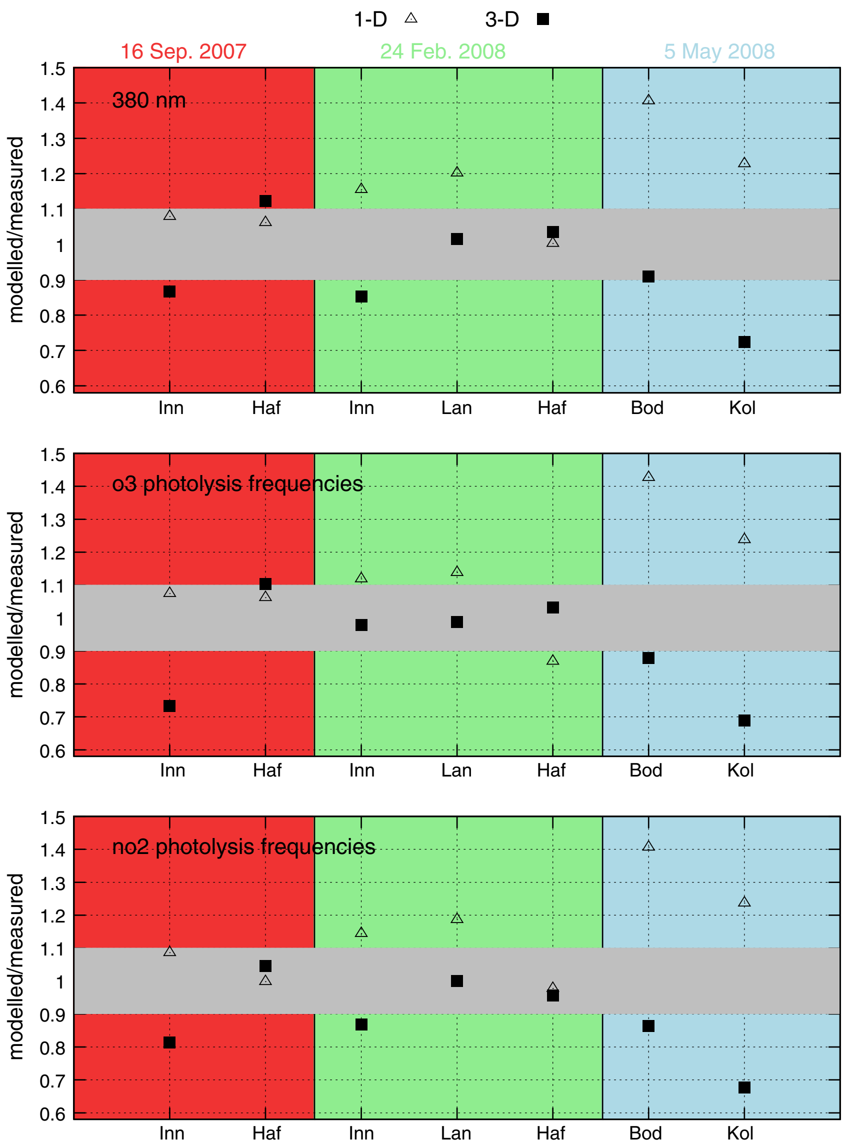

Fig. 4. Same as Fig. 3 but for 380 nm and photolysis frequencies. Top - 380 nm, center - O3 photolysis frequencies, bottom - NO2 photolysis frequencies.

contribute to photolysis frequencies and one can add "photons" from different wavelengths to obtain photolysis frequencies.

3. Results and discussion

3.1. Comparison of model results and measurements

Figs. 3 and 4 show the ratio of model calculations to the measurements. It is shown that the 3-D-model calculations (black filled squares) have a similar site to site variation as the 1-D-model calculations (black open triangles). Further there is a significant variation in the ratios for different stations and on different dates but spectrally the results for each site are self-consistent. This indicates that the correct wavelength dependent model input parameters (e.g. total ozone column) are used in the models. Therefore this implies that changes in the ratios on different days are mainly due to real changes in the snow cover which cause changes in the agreement between the actual and the model snow-cover. The local topography of the station (valley, mountain top) also has a significant impact. The simulations using the 3-D-model are significantly closer to the measurements on 5th May 2008 especially for *Bod* station. The results suggest for *Bod* and *Kol* (both located in a steep valley), that obstructions on the horizon results in a decrease in actinic flux at both stations. The 1-D-model cannot take this phenomenon into account whereas the 3-Dmodel includes the effect of topography and thus more accurately reproduce the measurements. However in the case of *Kol*, this effect is overestimated in the 3-D-model.

For 16th September 2007 the 1-D-model reproduces the measurements better than the 3-D-model. For this day the 3-D-model significantly underestimates actinic flux for station *Inn* and slightly overestimates actinic flux for the station *Haf*. The agreement between 1-D-model results and measurements is surprisingly good and interestingly consideration of topography within the 3-D-model does not improve the results.

On 24th February the 3-D-model generally reproduces the measurements better than the 1-D-model for the valley stations *Inn* and *Lan*. The ratios of both models for the mountain top station *Haf* are similar.

The results suggest that in cases with less snow cover (16th September 2007 and 24th February 2008) the 1-D-model is able to reproduce the measurements to within 20% (Figs. 3 and 4). This result was expected, since multiple reflections on inhomogeneous surfaces are reduced by low surface albedo and the 1-D approximation works quite well. In general the 1-D-model agrees better with measurements at the mountain station (Haf) where the situation is closest to a site with a clear horizon. In situations with significant snow cover and a steep valley (5th May 2008) the 1-D-model does not agree well with the measurements. Under such conditions one expects a large impact of surface scattered radiation, highly influenced by topography, which cannot be properly taken into account in the 1-D-model. For these cases the 3-Dmodel reproduces the interaction between high surface albedo and topography better. However, at Kol the 3-D-model tends to overestimate the obstruction of the horizon, possibly due to an error in estimation of the snowline which was between the two sites *Bod* and *Kol*.

3.2. Influence of topography and surface albedo

The topography used in the 3-D-model is shown in Figs. 1 and 2 and the spatial distribution of spectral actinic flux for 324 nm is shown for two different days (24th February 2008 and 5th May 2008) and areas (Figs. 7 and 5). Apart from minor boundary problems (e.g. mountain shadow at the Southern boundary in Fig. 7), the typical features of radiation in mountainous areas are well reproduced with the actinic flux increasing with altitude. We observed an increase of about 15% 1000 m at 305 nm and about 5% at 400 nm. However the increase can vary a lot depending both on location and solar zenith angle (see Figs. 1, 2, 5 and 7), with the highest values occuring on south-facing slopes. Due to the high solar zenith angle on 24th February, the steepest parts of the north-facing slopes are shaded, resulting in significantly lower actinic flux values (Fig. 7). This feature is not visible in Fig. 5 where the solar zenith angle is 29.67°. The greatest values in both cases (Figs. 5 and 7) occur on south-facing snow-covered slopes in narrow valleys.

To study the influence of snow in combination with topography on surface actinic flux we performed additional calculations without snow using the 3-D-model. The results show that snow cover in combination with topography can significantly enhance actinic flux in some areas (up to 25%, see Figs. 6 and 8). Surprisingly the effect of snow is almost negligible in the snow-free valley bottom. The snowline within the model was at 1700 m for the south-facing and at 1300 m for the north-facing slopes. Although the distance between valley and snow-covered mountain slopes is small, e.g. about 5 km between Innsbruck and the snow-covered Nordkette (mountains north of Innsbruck), the snow-covered mountains don't significantly increase the actinic flux at the valley site in Innsbruck.

To determine 3-D-effects we run the 1-D-model was run for each pixel of the Innsbruck area 3-D model domain with surface height and albedo being taken from the 3-D-model.

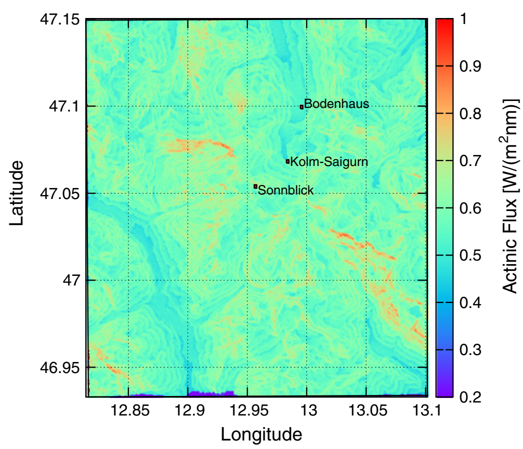

Fig. 5. Calculated actinic flux F_λ from the 3-D model on 05/07/2008 for 324 nm 11:18 UTC with realistic surface albedo (with snow), position of the sun is at 29.67 zenith angle and 186.52 azimuth angle.

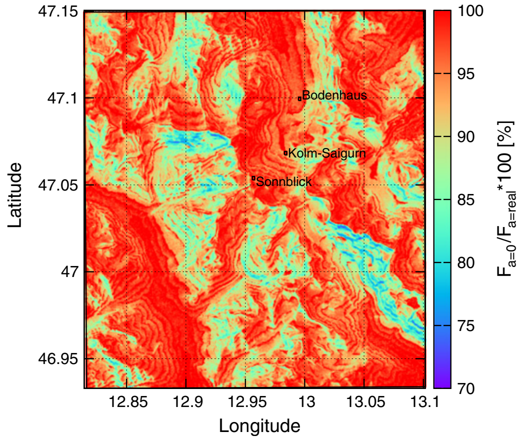

Fig. 6. Ratio of calculated actinic flux with black surface ($F_{a=0}$) and calculated actinic flux with realistic surface albedo ($F_{a=real}$) for 324 nm 11:18 UTC, position of the sun is at 29.67 degree zenith angle and 186.52 azimuth angle.

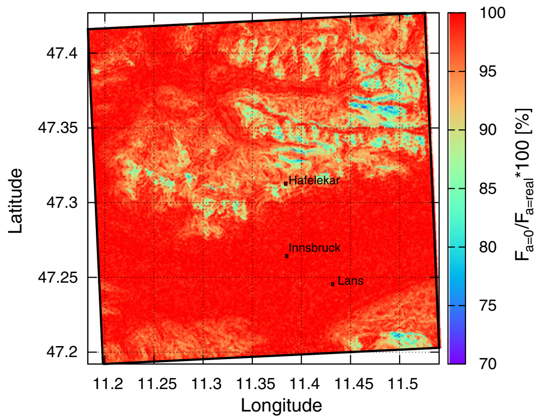

Fig. 8. Same as Fig. 6 but for Innsbruck area on 24/02/2008 11:17 UTC, position of the sun is at 56.92 zenith angle and 198.63 azimuth angle.

The ratio of spectral actinic flux at 324 nm calculated with the 3-D-model to the 1-D-model results is shown in Fig. 9. Red and yellow indicate where the 3-D-model calculates higher values than the 1-Dmodel, green and blue mark regions where 3-D-model results are lower than those of the 1-D-model. The snowline is clearly visible (border between red and green), here surface albedo jumps from 0.03 to 0.7 with altitude resulting in a jump in actinic flux within the 1-D-model of about 40%. In the 3-D-model the change over from snow-free to snow-covered areas results in a much smoother increase of actinic flux. Therefore we observe ratios up to 130% in snow-free areas close to snow-covered areas and ratios of around 80% in snow-covered areas close to snow-free areas. Blue areas with ratios below 60% indicate shaded regions (only diffuse radiation in the 3-Dmodel, but direct and diffuse radiation in the 1-D-model). From these results one could estimate an effective albedo for each pixel. Running the 1-D-model with such an albedo value would result in the same value as the 3-D-model. In this way one could incorporate 3-D-effects in a 1-D-model (and benefit from 1-D-model advantages such as being user friendly and computationally faster). However, at present the differences between the 3-D-model results and the measurements (Figs. 3 and 4) are too large for such an approach.

Overall the results suggest that topography has a large impact on the actinic flux field. Generally a rugged topography tends to reduce actinic flux in comparison with a flat topography. On the other hand the impact of snow on the ground is less pronounced than expected. It seems that the steep mountain sides which have an albedo of 0.03 below 1300 m/1700 m (north-facing and south-facing slopes respectively) act as a barrier to light reflected from the surface.

4. Conclusions and outlook

In general 1-D-model calculations are not able to reproduce spectral actinic flux and photolysis frequencies in complex Alpine terrain under cloud-free conditions within the desired accuracy of about 10%. Furthermore it is not possible to derive realistic 2-D-surface actinic flux fields with 1-D-models. In this case study the 1-D-model simulations showed a significant overestimation of actinic fluxes. Since crucial atmospheric parameters like total column ozone, ozone profile, aerosol optical depth and aerosol profiles are

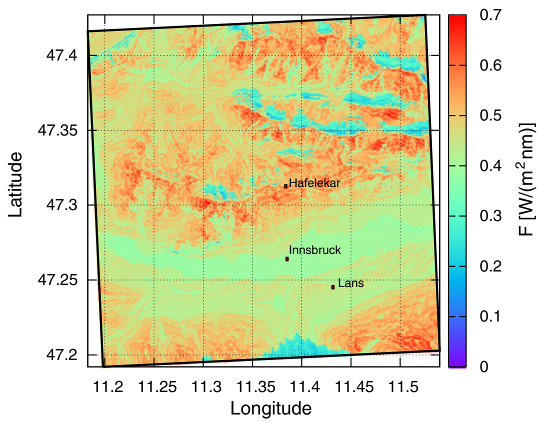

Fig. 7. Same as Fig. 5 but for Innsbruck area on 24/02/2008 11:17 UTC, position of the sun is at 56.92 zenith angle and 198.63 degree azimuth angle.

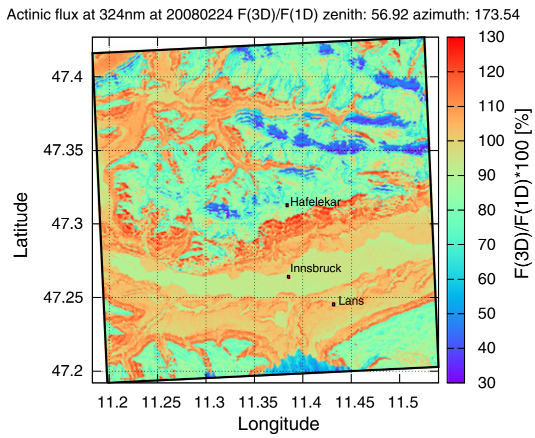

Fig. 9. Ratios of actinic flux calculated with 3-D-model and 1-D-model.

known with reasonable accuracy, the observed deviation between model results and observations are most likely resulting from 3-D effects. However, the modified 3-D-model was also not able to reproduce actinic flux measurements to within the 10% accuracy. The 3-D-model gave significantly different results from the 1-D-model and in general underestimated actinic flux. Overall the accuracy of the 3-D-model was of the same order as the 1-D-model, we conclude that topography generally tends to significantly reduce actinic flux in situations with moderate snow cover (average surface albedo in our cases was between 0.14 and 0.59), which implies it is very important to take topography into account if one is interested in actinic flux in mountainous terrain. However, a big source of uncertainty remains in the determination of the surface albedo. In our study only two different values for surface albedo were used, one for snow-covered areas and one for snow free areas (Table 2). More detailed surface albedo information (e.g. from land use maps) is needed to improve the 3-D-model calculations. Furthermore one should address the problem of different geometries. The entrance optic used for the measurements is a hemispheric sampling head (2 π response), but within the 3-D-model the “photons” are counted on five surfaces of a cuboid. It would be useful to determine if any significant errors result from this difference. Despite these limitations, our 3-D-model calculations allow us to estimate the potential impact of surface albedo on actinic flux. The results indicate that the influence of surface albedo can vary greatly depending on the area considered from being a very important effect (e.g. in steep valleys), to only a minor influence (e.g. bottom of wide valleys).

Acknowledgments

The authors would like to thank the referees for helpful advice and comments. This work was financed by FWF Austrian Research Fund within the project “Investigation of actinic flux in mountainous areas under cloudless conditions”, project number: P18780-N13.

Appendix A

For each pixel i the photon number N(i) has to be converted to actinic flux $F(i)$. Thus we can state:

$$F(i) = N(i)K(i)\xi(i) \tag{2}$$

where $\xi(i)$ is a correction factor according to pixel discontinuities within the model and $K(i)$ is the conversion factor between photon number and actinic flux. From geometrical reasons follows:

$$K(i) = \frac{I_{ext}cos(\theta)CA}{A_p(i)N} \tag{3}$$

with I_{ext} - extraterrestrial Irradiance, A - surface area of the whole model domain, C - correction factor due to varying sun-earth distance, N - total number of photons and $Ap(i)$ - area of the projected facet (perpendicular to the incident beam) of the cuboid used for counting photons. The calculation of Ap (i) is rather complex and depend on the geometry of the cuboid and the position of the sun. We split the calculation into the direct beam (index ^{dir}) and the diffuse radiation (index ^{dif})

$$A_p^{dir}(i) = z(i)sin(\theta)y(i)sin(\phi) + z(i)sin(\theta)x(i)cos(\phi) + x(i)y(i)cos(\theta) \tag{4}$$

with x, y, z -length, width and height of the cuboid, θ - zenith angle and ϕ azimuth angle. With this approach the projected facet for the direct beam can be calculated. With the assumption of isotrophy, the projected facet for diffuse radiation $A_p^{dif}(i)$ can be calculated by integration of $A_p^{dif}(i)$ over the hemisphere:

$$A_p^{dif}(i) = \frac{1}{2\pi}\int_0^{2\pi}\int_0^{\pi/2} sin\theta A_p^{dir}(i)d\theta d\phi \tag{5}$$

The normalized projected facet for different cuboid geometries dependent on zenith angle are shown in Fig. 1. Since the normalized projected facet also depends on the azimuth angle, an area is shown for each cuboid. The lower boundary of the colored area (see legend in graph) corresponds to azimuth angle of 0 and the upper boundary to an azimuth angle of 45. To convert direct photon numbers into actinic flux for each simulation the projected facet (A_p) was calculated (colored dots in the graph). A_p^{diff} is also shown in Fig. 10 (thin coloured horizontal lines).

For the determination of the pixel discontinuity error, again we distinguish between direct radiance and diffuse radiance. For radiation coming directly from the sun, the error estimate is straight forward. For a situation without an atmosphere (no scattering, no absorption) one can calculate the theoretical photon number at each pixel $N_{dir}(i)$:

$$N_{dir}(i) = \frac{A_p(i)N}{Acos\theta} \tag{6}$$

We performed a reference simulation with the 3-D-model with photons hitting the top of the model at a random point with fixed zenith and azimuth angle according to the position of the sun and thus we calculated also for each pixel a photon number $N_{dir}^{3D}(i)$. The discontinuity correction factor for direct radiation is the ratio:

$$\xi_{dir}(i) = \frac{N_{dir}(i)}{N_{dir}^{3D}(i)} \tag{7}$$

For diffuse radiation (with the assumption of isotropic distribution) the calculation is more complex. One has to take into account the obstruction of the horizon H (i) to calculate the theoretical photon number at each pixel for a situation without atmosphere:

$$N_{dif}(i) = \frac{A_p(i)N}{A * 0.638139}H(i) \tag{8}$$

0.638139 is the average cosine of the angle of incident and $H(i)$ is the proportion of not obstructed actinic flux (value between 1 - unobstructed and 0 - fully obstructed) with

$$H(i) = \frac{1}{2\pi A_p^{dif}(i)}\int_0^{2\pi}\int_0^{\pi/2} sin\theta A_p^{dir}(i)f(i,\theta,\phi)d\theta d\phi \tag{9}$$

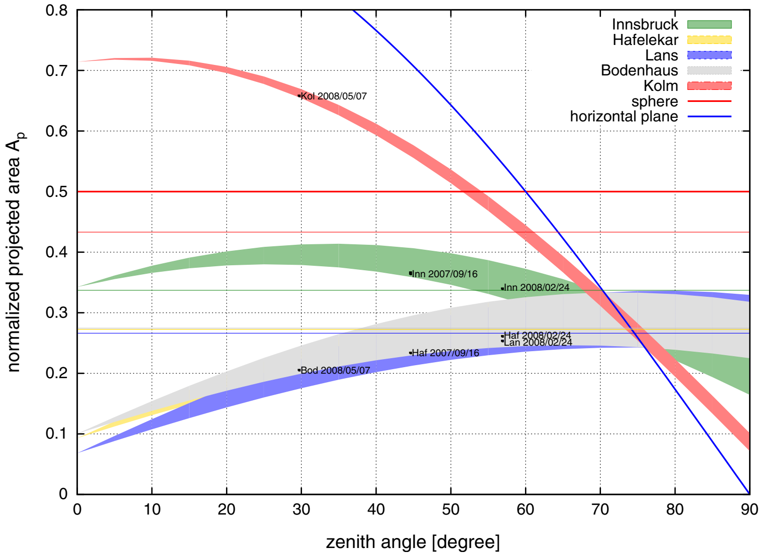

Fig. 10. Normalized projected facet of the five cuboids at the measurement sites Innsbruck (Inn), Lans (Lan), Hafelekar (Haf), Bodenhaus (Bod) and Kolm-Saigurn (Kol) within the model domain. Thin colored horizontal lines indicate the normalized diffuse projected facet (A_p^{diff}) for each measurement site, black dots indicate direct normalized projected facet (A_p^{dir}) for each measurement site and date.

$f(i,\theta,\phi)$ is a simple numerical factor to account for the obstruction of the horizon. If the sky is obstructed at a certain position $f(i,\theta,\phi)$ is equal to 0 otherwise $f(i,\theta,\phi$ is equal 1. f is calculated prior to the calculation of H by a routine which calculated the obstruction of the horizon for each azimuth angle taking into account the surrounding pixels altitude and the central pixel inclination and orientation. It works using a virtual beam which“scans”the horizon.

We performed a second reference simulation with the 3-D-model with photons enter the top of the model with random zenith and random azimuth angle to calculate photon numbers for each pixel $N_{dif}^{3D}(i)$. Again we use the ratio of the theoretical approach to the model calculation to derive the discontinuity correction factor:

$$\xi_{dif}(i) = \frac{N_{dir}(i)}{N_{dif}^{3D}(i)} \tag{10}$$

References

Anderson, G., Clough, S., Kneizys, F., Chetwynd, J., Shettle, A., 1986. AFGL atmospheric constituent profiles (0–120 km). Technical Report AFGL-Tr-86-110. Air Force Geophysics Laboratory, Hanscom Air Force Base, Bedford, MA.

Angelini, F., Barnaba, F., Landi, T., Caporaso, L., Gobbi, G., 2009. Study of atmospheric aerosols and mixing layer by lidar. Radiation Protection Dosimetry. doi:10.1093/rpd/ncp219.

Ångstrøm, A., 1929. On the atmosperic transmission of sun radiation and on dust in the air. Geografiska Annaler 11, 156–166.

Bais, A., Gardiner, B., Slaper, H., Blumthaler, M., Bernhard, G., McKenzie, R., Webb, A., Seckmeyer, G., Kjeldstad, B., Koskela, T., Kirsch, P., Gr¨obner, J., Kerr, J., Kazadzis, S., Leszczynski, K., Wardle, D., Josefsson, W., Brogniez, C., Gillotay, D., Reinen, H., Weihs, P., Svenoe, T., Eriksen, P., Kuik, F., Redondas, A., 2001. Suspen intercomparison of ultraviolet spectroradiometers. Journal of Geophysical Research D: Atmospheres 106, 12509–12525 Cited By (since 1996) 57.

Bais, A.F., Madronich, S., Crawford, J., Hall, S.R., Mayer, B., van Weele, M., Lenoble, J., Calvert, J.G., Cantrell, C.A., Shetter, R.E., Hofzumahaus, A., Koepke, P., Monks, P.S., Frost, G., McKenzie, R., Krotkov, N., Kylling, A., Swartz, W.H., Lloyd, S., Pfister, G., Martin, T.J., Roeth, E., Griffioen, E., Ruggaber, A., Krol, M., Kraus, A., Edwards, G.D., Mueller, M., Lefer, B.L., Johnston, P., Schwander, H., Flittner, D., Gardiner, B.G., Barrick, J., Schmitt, R., 2003. International photolysis frequency measurement and model intercomparison (ipmmi): Spectral actinic solar flux measurements and modeling. Journal of Geophysical Research D: Atmospheres 108.

Bass, L., Nikolaeva, O., Kuznetsov, V., Kokhanovsky, A., 2010. Radiation balance in a cloudy atmosphere with account for the 3D effects. Atmospheric Research 98, 1–8 Clouds, Aerosols and Radiation - EGU09.

Bernhard, G., Seckmeyer, G., 1999. Uncertainty of measurements of spectral solar uv irradiance. Journal of Geophysical Research D: Atmospheres 104, 14321–14345.

Bierwirth, E., Wendisch, M., Jkel, E., Ehrlich, A., Schmidt, K.S., Stark, H., Pilewskie, P., Esselborn, M., Gobbi, G.P., Ferrare, R., Mller, T., Clarke, A., 2010. A new method to retrieve the aerosol layer absorption coefficient from airborne flux density and actinic radiation measurements. Journal of Geophysical Research D: Atmospheres 115.

Blumthaler, M., Ambach, W., 1988. Solar UVB-albedo of various surfaces. Photochemistry and Photobiology 48, 85–88.

Burrows, W., 1997. CART regression models for predicting UV radiation at the ground in the presense of cloud and other environmental factors. Journal of Applied Meteorology 36, 531–544.

Cahalan, R.F., Oreopoulos, L., Marshak, A., Evans, K.F., Davis, A., Pincus, R., Yetzer, K., Mayer, B., Davies, R., Ackerman, T., Barker, H., Clothiaux, E., Ellingson, R., Garay, M., Kassianov, E., Kinne, S., Macke, A., OHirok, W., Partain, P., Prigarin, S., Rublev, A., Stephens, G., Szczap, F., Takara, E., Varnai, T., Wen, G., Zhuravleva, T., 2005. The International Intercomparison of 3D Radiation Codes (I3RC): Bringing together the most advanced radiative transfer tools for cloudy atmospheres. Bulletin of the American Meteorological Society 86 (9), 1275–1293.

Dahlback, A., Stamnes, K., 1991. A new spherical model for computing the radiation field available for photolysis and heating at twilight. Planetary and Space Science 39 (5), 671–683.

Degünther, M., Meerkötter, R., Albold, A., Seckmeyer, G., 1998. Case study on the influence of inhomogeneous surface albedo on uv irradiance. Geophysical Research Letters 25, 3587–3590.

Deutschmann, T., Beirle, S., Frie, U., Grzegorski, M., Kern, C., Kritten, L., Platt, U., Prados-Romn, C., Pukite, J., Wagner, T., Werner, B., Pfeilsticker, K., 2011. The Monte Carlo atmospheric radiative transfer Model Mcartim: introduction and validation of Jacobians and 3D features. Journal of Quantitative Spectroscopy and Radiative Transfer 112, 1119–1137.

Erb, R., 1996. Measurements of Spectral Solar Ultraviolet Radiation on Top of the Zugspitze (2964 m a. s. l.), volume 42. Dr. W. Maraun, Wissenschafts-Verlag.

Evans, K., Stephens, G., 1991. A new polarized atmospheric radiative transfer model. Journal of Quantitative Spectroscopy and radiative Transfer 46 (4), 413–423.

Feister, U., Grewe, R., 1995a. Higher UV-radiation inferred from low ozone levels at northern latitudes in 1992 and 1993. Global and Planetary change 11, 25–34.
Feister, U., Grewe, R., 1995b. Spectral albedo measurements in the UV and VISIBLE region over different types of surfaces. Photochemistry and Photobiology 62, 736–744.
Gobbi, G., Barnaba, F., Van Dingenen, R., Putaud, J., Mircea, M., Facchini, M., 2003. Lidar and in situ observations of continental and Saharan aerosol: closure analysis of particles optical and physical properties. Atmospheric Chemistry and Physics 3, 2161–2172.
Hofzumahaus, A., Kraus, A., Mller, M., 1999. Solar actinic flux spectroradiometry: a technique for measuring photolysis frequencies in the atmosphere. Applied Optics 38, 4443–4460.
Hofzumhaus, A., Kraus, A., Kylling, A., Zerefos, C., 2002. Solar actinic radiation (280–420 nm) in the cloud-free troposphere between ground and 12 km altitude: measurements and model results. Journal of Geophysical Research 107 (D18). doi:10.1029/2001JD900142.
Jaroslawski, J.P., K.J., 2005. Importance of aerosol variations for surface UVB level: analysis of ground-based data taken at Belsk, Poland, 1992–2004. Journal of Geophysical Research-Atmospheres 110, D16201.
Junkermann, W., Platt, U., Volz-Thomas, A., 1989. A photoelectric detector for the measurement of photolysis frequencies of ozone and other atmospheric molecules. Journal of Atmospheric Chemistry 8, 203–227.
Kaczmarek, H., GaLka, P., Wrzyszczynski, A., Olszewski, K., Janota, H., 2009. Effect of new photoinitiator on the courses of photochemical reactions in poly (vinyl chloride). Polimery/Polymers 54, 202–208.
Kerr, J., 2003. Understanding the factors that affect surface UV radiation. Proceedings of SPIE 5156, pp. 1–14.
Kylling, A., Mayer, B., 2001. Ultraviolet radiation in partly snow covered terrain: observations and three-dimensional simulations. Geophysical Research Letters 28 (19), 3365–3368.
Kylling, A., Bais, A.F., Blumthaler, M., Schreder, J., Zerefos, C.S., Kosmidis, E., 1998. Effect of aerosols on solar UV irradiances during the Photochemical Activity and Solar Ultraviolet Radiation campaign. Journal of Geophysical Research 103, 26051–26060.
Kylling, A., Dahlback, A., Mayer, B., 2000. The effect of clouds and surface albedo on UV irradiances at a high latitude site. Geophysical Research Letters 27, 1411–1414.
Kylling, A., Webb, A.R., Bais, A.F., Blumthaler, M., Schmitt, R., Thiel, S., Kazantzidis, A., Kift, R., Misslbeck, M., Schallhart, B., Schreder, J., Topaloglou, C., Kazadzis, S., Rimmer, J., 2003. Actinic flux determination from measurements of irradiance. Journal of Geophysical Research D: Atmospheres 108.
Kylling, A., Webb, A., Kift, R., Gobbi, G., Ammannato, L., Barnaba, F., Bais, A., Kazadzis, S., Wendisch, M., J¨ackel, E., Schmidt, S., Kniffka, A., Thile, S., Junkermann, W., Blumthaler, M., Silbernagl, R., Schallhart, B., Schmitt, R., Kjeldstad, B., Thorseth, T., Scheirer, R., Mayer, B., 2005. Spectral actinic flux in the lower troposphere: measurement and 1-D simulations for cloudless, broken cloud and overcast situations. Atmospheric Chemistry and Physics 5, 1975–1997.
Lenoble, J., Kylling, A., Smolskaia, I., 2004. Impact of snow cover and topography on ultraviolet irradiance at the alpine station of brianon. Journal of Geophysical Research D: Atmospheres 109.
Madronich, S., 1987. Photodissociation in the atmosphere, 1. Actinic flux and the effects on ground reflection and clouds. Journal of Geophysical Research 92, 9740–9752.
Mayer, B., Kylling, A., 2005. Technical note: the LibRadtran software package for radiative transfer calculations — description and example of use. Atmospheric Chemistry and Physics 5, 1855–1877.
McKenzie, R., Kotkamp, M., Seckmeyer, G., Erb, R., Roy, C., Gies, H., Toomey, S., 1993. First southern hemisphere intercomparison of measured solar UV spectra. Geophysical Research Letters 20 (20), 2223–2226.
Melamed, M.L., Michos, E.D., Post, W., Astor, B., 2008. 25-hydroxyvitamin d levels and the risk of mortality in the general population. Archives of Internal Medicine 168, 1629–1637 (Cited By (since 1996): 142).
Palancar, G.G., Shetter, R.E., Hall, S.R., Toselli, B.M., Madronich, S., 2011. Ultraviolet actinic flux in clear and cloudy atmospheres: model calculations and aircraft-based measurements. Atmospheric Chemistry and Physics Discussions 11, 3321–3354.
Paur, Bass, 1985. The ultraviolet cross section of ozone, ii, results and temperature dependence. Atmospheric Ozone, proceedings of the Quadrennial Ozone Symposium. Halkidiki, Greece.
Pribullova, A., Chmelik, M., 2008. Typical distribution of the solar erythemal uv radiation over Slovakia. Atmospheric Chemistry and Physics 8, 5393–5401.
Raff, J.D., Finlayson-Pitts, B.J., 2010. Hydroxyl radical quantum yields from isopropyl nitrite photolysis in air. Environmental Science and Technology 44, 8150–8155.
Rieder, H., Staehelin, J., Weihs, P., Vuilleumier, L., Maeder, J., Holawe, F., Blumthaler, M., Lindfors, A., Peter, T., Simic, S., Spichtinger, P., Wagner, J., Walker, D., Ribatet, M., 2010. Relationship between high daily erythemal UV doses, total ozone, surface albedo and cloudiness: an analysis of 30 years of data from Switzerland and Austria. Atmospheric Research 98, 9–20 (Clouds, Aerosols and Radiation - EGU09).
Scheirer, R., Macke, A., 2001. On the accuracy of the independent column approximation in calculating the downward fluxes in the UVA, UVB and PAR spectral ranges. Jounal of Geophysical Research 106 (D13), 14301–14312.
Scheirer, R., Macke, A., 2003. Cloud inhomogeneity and broadband solar flux. Journal of Geophysical Research 108 (D19). doi:10.1029/2002JD003321.
Schmalwieser, A.W., Erbertseder, T., Schauberger, G., Weihs, P., 2008. Sensitivity of UV erythemally effective irradiance and daily dose to spatial variability in total ozone. Photochemistry and Photobiology 84, 1149–1163.
Schwander, H., Mayer, B., Ruggaber, A., Albold, A., Seckmeyer, G., Koepke, P., 1999. Method to determine snow albedo values in the ultraviolet for radiative transfer modeling. Applied Optics 38 (18), 3869–3875.
Simic, S., Weihs, P., Kromp-Kolb, H., Vacek, A., Laube, W., 2005. Factors affecting changes of spectral UV irradiance at the Sonnblick Observatory (3106 m, Austria). Proceedings SPIE 59, 79271–79279.
Simic, S., Weihs, P., Vacek, A., Kromp-Kolb, H., Fitzka, M., 2008. Spectral UV measurements in Austria from 1994 to 2006: investigations of short- and long-term changes. Atmospheric Chemistry and Physics 8, 7033–7043.
Slaper, H., R.H., Blumthaler, M., Huber, M., Kuik, F., 1995. Comparing ground-level spectrally resolved solar UV measurements using various instruments: a technique resolving effects of wavelength shift and slit width. Geophysical Research Letters 22 (20), 2721–2724.
Stamnes, K., Tsay, S., Wiscombe, W., Jayaweera, K., 1988. Numerically stable algorithm for discrete-ordinate-method radiative transfer in multiple scattering and emitting layered media. Applied Optics 27, 2502–2509.
Thiel, S., Ammannato, L., Bais, A., Bandy, B., Blumthaler, M., Bohn, B., Engelsen, O., Gobbi, G.P., Grobner, J., Jnkel, E., Junkermann, W., Kazadzis, S., Kift, R., Kjeldstad, B., Kouremeti, N., Kylling, A., Mayer, B., Monks, P.S., Reeves, C.E., Schallhart, B., Scheirer, R., Schmidt, S., Schmitt, R., Schreder, J., Silbernagl, R., Topaloglou, C., Thorseth, T.M., Webb, A.R., Wendisch, M., Werle, P., 2008. Influence of clouds on the spectral actinic flux density in the lower troposphere (INSPECTRO): overview of the field campaigns. Atmospheric Chemistry and Physics 8, 1789–1812.
Volz-Thomas, A., Lerner, A., Ptz, H., Schultz, M., McKenna, D., Schmitt, R., Madronich, S., Röth, E.P., 1996. Airborne measurements of the photolysis frequency of no2. Journal of Geophysical Research D: Atmospheres 101, 18613–18627.
Webb, A.R., Bais, A.F., Blumthaler, M., Gobbi, G., Kylling, A., Schmitt, R., Thiel, S., Barnaba, F., Danielsen, T., Junkermann, W., Kazantzidis, A., Kelly, P., Kift, R., Liberti, G.L., Misslbeck, M., Schallhart, B., Schreder, J., Topaloglou, C., 2002. Measuring spectral actinic flux and irradiance: experimental results from the admira (actinic flux determination from measurements of irradiance). Journal of Atmospheric and Oceanic Technology 19, 1049–1062.
Weihs, P., Simic, S., Laube, W., Mikielewicz, W., Rengarajan, G., Mandl, M., 1999. Characteristics of clear sky surface UV irradiance at high mountain observatory Sonnblick (3106 m altitude). Journal of Applied Meteorology 38 (11), 1599–1610.
Weihs, P., Lenoble, J., Blumthaler, M., Martin, T., Seckmeyer, G., Philipona, R., De la Casiniere, A., Sergent, C., Gröbner, J., Cabot, T., Masserot, D., Pichler, T., Pougatch, E., Rengarajan, G., Schmucki, D., Simic, S., 2001. Modeling the effect of an inhomogeneous surface albedo on incident UV radiation in mountainous terrain: determination of an effective surface albedo. Geophysical Research Letters 28, 3111–3115.